Surf. Sci. Spectra, 28(2) Dec 2021; doi: 10.1116/6.0001146 - Published under an exclusive license by the AVS

Analysis of Co_3O_4-SnO_2 and Co_3O_4-Fe_2O_3 nanosystems by X-ray photoelectron spectroscopy

Chiara Maccato,[1] Lorenzo Bigiani,[1] Max Klotzsche,[1] Davide Barreca,[2,a)] and Alberto Gasparotto[1]

[1] *Department of Chemical Sciences, Padova University and INSTM, 35131 Padova, Italy*

[2] *CNR-ICMATE and INSTM, Department of Chemical Sciences, Padova University, 35131 Padova, Italy*

(Received day Month year; accepted day Month year; published day Month year)

In this work, X-ray photoelectron spectroscopy (XPS) was employed to characterize the surface composition and elemental chemical states of supported Co_3O_4-SnO_2 and Co_3O_4-Fe_2O_3 nanocomposites. The present materials were prepared on Si(100) substrates by the chemical vapor deposition (CVD) of cobalt oxide under O_2+H_2O atmospheres, followed by the tailored introduction of SnO_2 or Fe_2O_3 by means of radio frequency (RF)-sputtering. Material structural and morphological characterization revealed the formation of nanocomposite heterostructures involving a conformal Co_3O_4 coverage by SnO_2 or Fe_2O_3 overlayers. Survey spectra, as well as detailed scans of C1s, O1s, Co2p, Sn3d and Fe2p regions are presented and critically discussed. The results provide evidence for the formation of pure and oxygen-deficient nanocomposites, and the occurrence of an electronic interplay between the single oxide constituents.

Keywords: Co_3O_4; SnO_2; Fe_2O_3; CVD; RF-sputtering; X-ray photoelectron spectroscopy

Acccession#: Enter Accession Number.

Technique: XPS

Host Material: Co_3O_4-SnO_2; Co_3O_4-Fe_2O_3

Instrument: Perkin-Elmer Physical Electronics, Inc. 5600ci

Major Elements in Spectra: C, O, Co, Sn, Fe

Minor Elements in Spectra: none

Published Spectra: 10

Spectra in Electronic Record: 10

Spectral Category: comparison

INTRODUCTION

Among metal oxides, cobalt oxide (Co_3O_4), a versatile *p*-type semiconductor endowed with a band gap enabling to efficiently harvest visible light, has received attention as an attractive material for different (photo)catalytic applications (Refs. 1-9). Nevertheless, to the best of our knowledge, no works focusing on Co_3O_4-based materials as photocatalysts for the removal of atmospheric nitrogen oxides (De-NO_x) are available in the literature up to date. Indeed, this kind of technological application has been the focus of an ever growing interest for the protection of both environment and human health, since nitrogen monoxide (NO) can yield various problems including photochemical smog, acid rains, and ozone depletion, detrimentally affecting people health even at low concentrations (Refs. 3, 10-14). These issues, along with the high toxicity even of nitrogen dioxide (NO_2), have stimulated research efforts aimed at the fabrication of efficient and stable solar-active photocatalysts for air purification, especially in urban/industrialized areas (Refs. 15-17). In this regard, a key requirement is the obtainment of an enhanced selectivity towards the formation of harmless nitrate species as the main products (Refs. 15, 16, 18).

In our research group, the attention has been dedicated to the design and preparation of supported oxide nanosystems as De-NO_x photocatalysts, which are more promising than the conventionally studied powdered homologues thanks to their higher stability upon prolonged operation and easier recovery after use (Refs. 12, 19, 20). In this context, recent research activities have been focused on De-NO_x photocatalysts based on Co_3O_4 nanomaterials obtained by chemical vapor deposition (CVD), an attractive route for the preparation of supported materials with tailored properties (Ref. 14). Furthermore, we have explored the influence of Co_3O_4 functionalization with SnO_2 or Fe_2O_3 for a possible tailoring of the ultimate system photoactivity. Whereas SnO_2, exploited as environmental photocatalyst in combination with Co_3O_4 (Refs. 7, 21), possesses matched band potentials with Co_3O_4 ones to yield an improved separation of photogenerated charge carriers (Ref. 22), Fe_2O_3 yields a promising photocatalytic activity in various processes (Refs. 14, 20, 23, 24). Following our previous studies on the fabrication of metal oxide composites (Refs. 1, 19, 20, 25), SnO_2 or Fe_2O_3 deposition on Co_3O_4 was carried out by radio frequency (RF)-sputtering under mild conditions. In this context, the present contribution is dedicated to the room temperature X-ray photoelectron spectroscopy (XPS) analysis, performed using a standard Mg Kα X-ray source, of Co_3O_4-SnO_2 and Co_3O_4-Fe_2O_3 nanomaterials on Si substrates. The attention was devoted to the analysis of C1s, O1s, Co2p, Sn3d and Fe2p core levels, with particular regard to the chemical states of the different elements and to the interplay between the components of the developed nanocomposites. The latter, with specific reference to electronic interactions, directly influences the ultimate material activity in photocatalytic De-NO_x applications. The results of this investigation can pave the way to future research developments on the tailored engineering of oxide-oxide interfaces for the production of improved environmental photocatalysts.

SPECIMEN DESCRIPTION (ACCESSION # 00000

Host Material: Co_3O_4-SnO_2

CAS Registry #: unknown

Host Material Characteristics: homogeneous; solid; polycrystalline; semiconductor; composite; Thin Film

Chemical Name: Cobalt (II,III) oxide – tin (IV) oxide

Source: specimen deposited on Si(100) by CVD of Co_3O_4 and subsequently functionalized with SnO_2 by RF-sputtering

Host Composition: Co, O, Sn

[a)] Author to whom correspondence should be addresses. e-mail: davide.barreca@unipd.it.

Surf. Sci. Spectra, 28(2) Dec 2021; doi: 10.1116/6.0001146 - Published under an exclusive license by the AVS

Form: Supported nanocomposite thin film

Structure: The system structure was preliminarily investigated by X-ray diffraction (XRD) analyses, which provided evidence for the presence of a single peak at $2\theta = 36.9°$, corresponding to (311) crystallographic planes of cubic Co_3O_4 (Ref. 26). The lack of appreciable peaks related to crystalline SnO_2 or mixed Co-Sn-O phases was related to the low SnO_2 loading (Refs. 25). Field emission-scanning electron microscopy (FE-SEM) analyses (see inset in figure # NFigA01) highlighted the occurrence of uniformly distributed columnar nanostructures (mean width = 50 nm; mean length = 930 nm), grown perpendicularly to the substrate surface. Transmission electron microscopy (TEM) data revealed a conformal coverage of Co_3O_4 aggregates by a partially continuous, amorphous SnO_2 overlayer, whose very low thickness (a few nm) prevented its clear observation by FE-SEM analyses.

History & Significance: The used cobalt molecular precursor, $Co(tfa)_2$•TMEDA (htfa = 1,1,1-trifluoro-2,4-pentanedione; TMEDA = *N,N,N',N'*-tetramethylethylenediamine), was prepared by reacting the ligands with Co(II) chloride in alkaline aqueous solution. Co_3O_4 deposition was performed by CVD using a home-made, cold-wall horizontal CVD apparatus. Si(100) substrates (MEMC®, Merano, Italy) were pre-cleaned by sonication in i-PrOH and CH_2Cl_2, and subsequently etched in a 2% HF solution in order to remove the native SiO_2 film. Growth processes were performed at 400°C for 2 h, using a total pressure of 10.0 mbar. The precursor was heated at 70°C in an external reservoir located in an oil bath, and its vapors were transported into the reaction chamber through heated gas lines by means of an electronic grade O_2 flow [rate = 100 standard cubic centimeters per minute (sccm)]. An additional O_2 flow (rate = 100 sccm) was delivered into the reactor through a separate inlet, after passing through a H_2O reservoir maintained at 35°C. Functionalization with SnO_2 was accomplished by RF-sputtering from Ar plasmas using a home-made two-electrode plasmochemical reactor (ν = 13.56 MHz). A tin target (Neyco®; purity = 99.99%; diameter = 5 cm; thickness = 2.0 mm) was fixed on the RF electrode, whereas Si-supported Co_3O_4 was mounted on the grounded one. Depositions were performed at 60°C for 90 min, using a RF-power of 10 W, an electronic grade Ar flow rate of 10 sccm, and a total pressure of 1.0 mbar.

As Received Condition: as grown

Analyzed Region: same as host material

Ex Situ Preparation/Mounting: Sample fixed on a grounded sample holder and introduced into the analysis chamber through a fast entry lock system.

In Situ Preparation: none

Charge Control: No flood gun was used during analysis.

Temp. During Analysis: 298 K

Pressure During Analysis: $<10^{-8}$ Pa

Pre-analysis Beam Exposure: 180 s.

SPECIMEN DESCRIPTION (ACCESSION # 00000

Host Material: Co_3O_4-Fe_2O_3

CAS Registry #: unknown

Host Material Characteristics: homogeneous; solid; polycrystalline; semiconductor; composite; Thin Film

Chemical Name: Cobalt (II,III) oxide – iron (III) oxide

Source: specimen deposited on Si(100) by CVD of Co_3O_4 and subsequently functionalized with Fe_2O_3 by RF-sputtering

Host Composition: Co, O, Fe

Form: Supported nanocomposite thin film

Structure: The sample XRD pattern was very similar to that of Co_3O_4-SnO_2 (see the previous accession). In line with these observations, FE-SEM analyses (see inset in figure # NFigB01) showed no appreciable morphological variations with respect to the previous specimen, and TEM results evidenced a uniform and very thin (≈1 nm) Fe_2O_3 layer over the Co_3O_4 deposit, whose structure corresponded to that of γ-Fe_2O_3 (Ref. 27).

History & Significance: CVD of Co_3O_4 was performed using the same pre-cleaned Si(100) substrate and experimental conditions reported for the previous accession. Functionalization with Fe_2O_3 was performed by RF-sputtering starting from an iron target (Alfa Aesar®; purity = 99.995%; 5×5 cm^2; thickness = 0.25 mm), using the same plasmochemical apparatus and operating conditions reported from the previous specimen. The only exceptions were the RF-power and sputtering time values, which were set at 20 W and 180 min, respectively.

As Received Condition: as grown

Analyzed Region: same as host material

Ex Situ Preparation/Mounting: Sample fixed on a grounded sample holder and introduced into the analysis chamber through a fast entry lock system.

In Situ Preparation: none

Charge Control: No flood gun was used during analysis.

Temp. During Analysis: 298 K

Pressure During Analysis: $<10^{-8}$ Pa

Pre-analysis Beam Exposure: 180 s.

INSTRUMENT DESCRIPTION

Manufacturer and Model: Perkin-Elmer Physical Electronics, Inc. 5600ci

Analyzer Type: spherical sector

Detector: Channeltron

Number of Detector Elements: 16

INSTRUMENT PARAMETERS COMMON TO ALL SPECTRA

■*Spectrometer*

Analyzer Mode: constant pass energy

Throughput (T=E^N): N=0

Excitation Source Window: 1.5 micron Al window

Excitation Source: Mg Ka

Source Energy: 1253.6 eV

Source Strength: 250 W

Source Beam Size: > 25000 μm x > 25000 μm

Signal Mode: multichannel direct

■*Geometry*

Incident Angle: 9°

Source-to-Analyzer Angle: 53.8˚

Emission Angle: 45˚

Specimen Azimuthal Angle: 0˚

Acceptance Angle from Analyzer Axis: 0˚

Analyzer Angular Acceptance Width: 14˚ × 14˚

■Ion Gun

Manufacturer and Model: PHI 04-303 A

Energy: 4000 eV

Current: 0.4 mA/cm2

Current Measurement Method: Faraday cup

Sputtering Species: Ar^+

Spot Size (unrastered): 250 μm

Raster Size: 2000 μm x 2000 μm

Incident Angle: 40 ˚

Polar Angle: 45 ˚

Azimuthal Angle: 111 ˚

Comment: differentially pumped ion gun

DATA ANALYSIS METHOD

Energy Scale Correction: -

Recommended Energy Scale Shift: 0 eV for both specimens

Peak Shape and Background Method: After performing a Shirley-type background subtraction (Ref. 28), BE and full width at half maximum (FWHM) values were determined by least-squares fitting adopting Gaussian/Lorentzian functions.

Quantitation Method: Atomic concentrations were calculated by peak area integration, using sensitivity factors provided by PHI V5.4A software.

ACKNOWLEDGMENTS

Padova University (DOR 2018–2020, P-DiSC#04BIRD2020-UNIPD EUREKA), AMGA Foundation (NYMPHEA project) and the INSTM Consortium (INSTM21PDBARMAC – ATENA, INSTM21PDGASPAROTTO - NANO^{MAT}) are acknowledged for financial support. Thanks are also due to Dr. L. Vanin (Department of Chemical Sciences, Padova University, Padova, Italy) for technical assistance.

REFERENCES

1. G. Carraro, C. Maccato, A. Gasparotto, K. Kaunisto, C. Sada, and D. Barreca, Plasma Processes Polym. **13**, 191 (2016).
2. L. Chen, X. Zuo, S. Yang, T. Cai, and D. Ding, Chem. Eng. J. **359**, 373 (2019).
3. J. Liu, X. Shi, H. Liu, L. Dong, and B. Li, Appl. Surf. Sci. **533**, 147498 (2020).
4. B. Yang, J. Liu, H. Qin, Q. Liu, X. Jing, H. Zhang, R. Li, G. Huang, and J. Wang, J. Alloys Compd. **727**, 52 (2017).
5. S.-S. Yi, B.-R. Wulan, J.-M. Yan, and Q. Jiang, Adv. Funct. Mater. **29**, 1801902 (2019).
6. S. Zhu, L.-a. Huang, Z. He, K. Wang, J. Guo, S.-e. Pei, H. Shao, and J. Wang, J. Electroanal. Chem. **827**, 42 (2018).
7. S. Agarwal, I. Tyagi, V. K. Gupta, M. Sohrabi, S. Mohammadi, A. N. Golikand, and A. Fakhri, Mater. Sci. Eng. C **70**, 178 (2017).
8. M. N. Rumyantseva, S. A. Vladimirova, N. A. Vorobyeva, I. Giebelhaus, S. Mathur, A. S. Chizhov, N. O. Khmelevsky, A. Y. Aksenenko, V. F. Kozlovsky, O. M. Karakulina, J. Hadermann, A. M. Abakumov, and A. M. Gaskov, Sens. Actuators, B **255**, 564 (2018).
9. X. Xu, X. Sun, H. Han, H. Peng, W. Liu, X. Peng, X. Wang, and X. Yang, Appl. Surf. Sci. **355**, 1254 (2015).
10. T. Shen, X. Shi, J. Guo, J. Li, and S. Yuan, Chem. Eng. J. **408**, 128014 (2021).
11. X. Song, G. Qin, G. Cheng, W. Jiang, X. Chen, W. Dai, and X. Fu, Appl. Catal., B **284**, 119761 (2021).
12. J. Hu, D. Chen, N. Li, Q. Xu, H. Li, J. He, and J. Lu, Appl. Catal., B **236**, 45 (2018).
13. X. Li, W. Zhang, W. Cui, J. Li, Y. Sun, G. Jiang, H. Huang, Y. Zhang, and F. Dong, Chem. Eng. J. **370**, 1366 (2019).
14. G. Carraro, R. Sugrañez, C. Maccato, A. Gasparotto, D. Barreca, C. Sada, M. Cruz-Yusta, and L. Sánchez, Thin Solid Films **564**, 121 (2014).
15. J. Balbuena, J. M. Calatayud, M. Cruz-Yusta, P. Pardo, F. Martín, J. Alarcón, and L. Sánchez, Dalton Trans. **47**, 6590 (2018).
16. J. Balbuena, M. Cruz-Yusta, and L. Sánchez, J. Nanosci. Nanotechnol. **15**, 6373 (2015).
17. R. Sugrañez, J. Balbuena, M. Cruz-Yusta, F. Martín, J. Morales, and L. Sánchez, Appl. Catal., B **165**, 529 (2015).
18. P. Chen, H. Liu, Y. Sun, J. Li, W. Cui, L. a. Wang, W. Zhang, X. Yuan, Z. Wang, Y. Zhang, and F. Dong, Appl. Catal., B **264**, 118545 (2020).
19. A. Gasparotto, G. Carraro, C. Maccato, C. Sada, J. Balbuena, M. Cruz-Yusta, L. Sánchez, N. Vodišek, U. Lavrencic Štangar, and D. Barreca, CrystEngComm **20**, 1282 (2018).
20. J. Balbuena, G. Carraro, M. Cruz, A. Gasparotto, C. Maccato, A. Pastor, C. Sada, D. Barreca, and L. Sánchez, RSC Adv. **6**, 74878 (2016).
21. P. Cheng, Y. Ni, K. Yuan, and J. Hong, Mater. Lett. **90**, 19 (2013).
22. R. Huang, S. Huang, D. Chen, Q. Zhang, T.-T. Le, Q. Wang, Z. Hu, and Z. Chen, J. Colloid. Interf. Sci. **542**, 460 (2019).
23. J. Balbuena, M. Cruz-Yusta, A. L. Cuevas, M. C. López-Escalante, F. Martín, A. Pastor, and L. Sánchez, RSC Adv. **6**, 92917 (2016).
24. J. Balbuena, M. Cruz-Yusta, A. L. Cuevas, F. Martín, A. Pastor, R. Romero, and L. Sánchez, J. Alloys Compd. **797**, 166 (2019).
25. L. Bigiani, D. Barreca, A. Gasparotto, T. Andreu, J. Verbeeck, C. Sada, E. Modin, O. I. Lebedev, J. R. Morante, and C. Maccato, Appl. Catal., B **284**, 119684 (2021).
26. Pattern N° 042-1467, JCPDS (**2000**).
27. ICSD card n° 247034.
28. D. A. Shirley, Phys. Rev. B **5**, 4709 (1972).
29. D. Briggs, and M. P. Seah, *Practical Surface Analysis: Auger and X-ray Photoelectron Spectroscopy* (John Wiley & Sons: New York, 2nd ed., 1990).
30. J. F. Moulder, W. F. Stickle, P. E. Sobol, and K. D. Bomben, *Handbook of X-ray photoelectron spectroscopy* (erkin Elmer Corporation, Eden Prairie, MN, USA, 1992).
31. L. Bigiani, D. Barreca, A. Gasparotto, and C. Maccato, Surf. Sci. Spectra **25**, 014003 (2018).
32. D. Meng, J. Si, M. Wang, G. Wang, Y. Shen, X. San, and F. Meng, Vacuum **171**, 108994 (2020).
33. X. Wang, and M. Gao, Nanoscale **10**, 12045 (2018).
34. Y. Zeng, H. Li, Y. Xia, L. Wang, K. Yin, Y. Wei, X. Liu, and S. Luo, ACS Appl. Mater. Interfaces **12**, 44608 (2020).
35. D. Barreca, A. Gasparotto, O. I. Lebedev, C. Maccato, A. Pozza, E. Tondello, S. Turner, and G. Van Tendeloo, CrystEngComm **12**, 2185 (2010).

Surf. Sci. Spectra, 28(2) Dec 2021; doi: 10.1116/6.0001146 - Published under an exclusive license by the AVS

36. J. Cai, S. Li, and G. Qin, Appl. Surf. Sci. **466**, 92 (2019).
37. Y. Xu, L. Zheng, C. Yang, X. Liu, and J. Zhang, Sens. Actuators, B **304**, 127237 (2020).
38. M. C. Biesinger, B. P. Payne, A. P. Grosvenor, L. W. M. Lau, A. R. Gerson, and R. S. C. Smart, Appl. Surf. Sci. **257**, 2717 (2011).
39. D. Barreca, S. Garon, E. Tondello, and P. Zanella, Surf. Sci. Spectra **7**, 81 (2000).

Surf. Sci. Spectra, 28(2) Dec 2021; doi: 10.1116/6.0001146. Published under an exclusive license by the AVS

SPECTRAL FEATURES TABLE

Spectrum ID #	Element/ Transition	Peak Energy (eV)	Peak Width FWHM (eV)	Peak Area (eV x cts/s)	Sensitivity Factor	Concentration (at. %)	Peak Assignment
NFigA02[a]	C1s	284.8	1.7	9546.4	0.296	20.7	Adventitious surface contamination
NFigA02[a]	C1s	286.3	2.0	2365.1	0.296	5.1	C-O species from precursor residuals
NFigA02[a]	C1s	288.5	2.3	1044.5	0.296	2.3	Adsorbed carbonates
NFigA03[b]	O1s	530.1	1.9	33452.4	0.711	29.6	Lattice oxygen in Co_3O_4 and SnO_2
NFigA03[b]	O1s	531.4	2.1	20329.0	0.711	18.1	Surface adsorbed –OH/ carbonate groups
NFigA04[c]	Co2p	…	…	45294	3.590	8.6	Co in Co_3O_4
NFigA04	$Co2p_{3/2}$	780.9	1.8	…	…	…	Co in Co_3O_4
NFigA04	$Co2p_{1/2}$	796.6	1.8	…	…	…	Co in Co_3O_4
NFigA05[d]	Sn3d	...		178484	…	15.6	Sn in SnO_2
NFigA05	$Sn3d_{5/2}$	486.7	1.4	108215	4.725	…	Sn in SnO_2
NFigA05	$Sn3d_{3/2}$	495.2	1.4	70269	…	…	Sn in SnO_2
NFigB02[a]	C1s	284.8	1.8	8834.6	0.296	21.7	Adventitious surface contamination
NFigB02[a]	C1s	286.5	1.9	1125.3	0.296	2.8	C-O species from precursor residuals
NFigB02[a]	C1s	288.5	2.1	1039.0	0.296	2.6	Adsorbed carbonates
NFigB03[b]	O1s	530.0	1.7	28863.1	0.711	29.5	Lattice oxygen in Co_3O_4 and Fe_2O_3
NFigB03[b]	O1s	531.4	2.2	18065.9	0.711	18.5	Surface adsorbed –OH/ carbonate groups
NFigB04[c]	Co2p	…	…	31137	3.590	6.4	Co in Co_3O_4
NFigB04	$Co2p_{3/2}$	780.7	2.1	…	…	…	Co in Co_3O_4
NFigB04	$Co2p_{1/2}$	796.3	2.1	…	…	…	Co in Co_3O_4
NFigB05[e]	Fe2p	...		73708	2.957	18.5	Fe in Fe_2O_3
NFigB05	$Fe2p_{3/2}$	711.0	3.5	…	…	…	Fe in Fe_2O_3
NFigB05	$Fe2p_{1/2}$	724.4	3.7	…	…	…	Fe in Fe_2O_3

[a] The sensitivity factor is referred to the whole C1s signal.
[b] The sensitivity factor is referred to the whole O1s signal.
[c] The sensitivity factor, peak area, and concentration are referred to the whole Co2p signal.
[d] Tin atomic percentage was evaluated basing on the area and sensitivity factor for the $Sn3d_{5/2}$ component reported in the next line.
[e] The sensitivity factor, peak area, and concentration are referred to the whole Fe2p signal.

Footnote to Spectra NFigA01 and NFigB01: Wide-scan spectra confirmed the functionalization of Co_3O_4 with SnO_2 and Fe_2O_3, with adventitious carbon as the only impurity. The surface presence of cobalt even after tin and iron oxide deposition was traced back to Co_3O_4 coverage by very thin SnO_2 and Fe_2O_3 overlayers.

Footnote to Spectra NFigA02 and NFigB02: For both specimens, the C1s peak could be fitted by means of three components, evidencing the presence of C species in different chemical environments. The most intense band, centered at 284.8 eV, was ascribed to adventitious contamination due to atmospheric exposure. A second component located at a mean BE of 286.4 was related to surface C-O moieties from precursor residuals, whereas the contribution at 288.5 eV was ascribed to adsorbed carbonates (Refs. 29-31). The C1s signal could be reduced to noise level after 5 min Ar^+ erosion, revealing a good purity of the target samples.

Footnote to Spectra NFigA03 and NFigB03: Two bands contributed to the O1s signal. The main component at BE ≈ 530.0 eV was attributed to lattice O, whereas the second one at BE = 531.4 eV was due to surface carbonates (Refs. 30, 31) and to -OH groups chemisorbed on oxygen defects (Refs. 5, 6, 8, 25, 32-34), which are reported to have a beneficial impact on material (photo)catalytic performances (Refs. 3, 6, 10, 11, 13, 18).

Footnote to Spectra NFigA04 and NFigB04: The Co2p peak shape and the absence of intense *shake-up* satellites, indicated the occurrence of Co_3O_4 as predominant phase (Refs. 2, 9, 25, 29, 33-35), in agreement with XRD results. The $Co2p_{3/2}$ BE was 780.9 and 780.7 eV for Co_3O_4-SnO_2 (**NFigA04**) and Co_3O_4-Fe_2O_3 (**NFigB04**) respectively, slightly higher values than those reported in the literature for bare Co_3O_4 (Refs. 1, 2, 30, 32, 36). This phenomenon was related to electronic interactions between the single oxides (Ref. 37), considering that, at the Co_3O_4/SnO_2 (Fe_2O_3) interface, an electron transfer occurs from Co_3O_4 to SnO_2 (Fe_2O_3) (see also comments to spectra **NFigA05** and **NFigB05**). The presence of weak Co2p shake-up satellites for Co_3O_4-Fe_2O_3 (**NFigB04**) may suggest the possible presence of CoO as a minority system component (Refs. 29, 35, 38), which may be undetectable by XRD analyses.

Footnote to Spectra NFigA05 and NFigB05: The Sn3d [$BE(Sn3d_{5/2})$ = 486.7 eV] and Fe2p [$BE(Fe2p_{3/2})$ = 711.0] peak position were slightly lower than previous literature data for SnO_2 (Refs. 9, 11, 29, 39) and Fe_2O_3 (Refs. 4, 14, 17, 23, 24, 36), respectively, supporting the above indicated electron transfer process (see comments to spectra **NFigA04** and **NFigB04**).
The average Sn/Co and Fe/Co atomic ratios were 1.8 and 2.9, respectively.

Surf. Sci. Spectra, 28(2) Dec 2021; doi: 10.1116/6.0001146 - Published under an exclusive license by the AVS

ANALYZER CALIBRATION TABLE

Spectrum ID #	Element/ Transition	Peak Energy (eV)	Peak Width FWHM (eV)	Peak Area (eV x cts/s)	Sensitivity Factor	Concentration (at. %)	Peak Assignment
figCalib01[a]	$Au4f_{7/2}$	84.0	1.4	186403	...	...	Au(0)
figCalib02[a]	$Cu2p_{3/2}$	932.7	1.6	86973	...	...	Cu(0)

[a] The peak was acquired after Ar^+ erosion.

GUIDE TO FIGURES

Spectrum (Accession) #	Spectral Region	Voltage Shift*	Multiplier	Baseline	Comment #
NFigA01	Survey	0	1	0	…
NFigA02	C 1s	0	1	0	…
NFigA03	O 1s	0	1	0	…
NFigA04	Co2p	0	1	0	…
NFigA05	Sn3d	0	1	0	…
NFigB01	Survey	0	1	0	…
NFigB02	C 1s	0	1	0	…
NFigB03	O 1s	0	1	0	…
NFigB04	Co2p	0	1	0	…
NFigB05	Fe2p	0		0	…

[*] Voltage shift of the archived (as measured) spectrum relative to the printed figure. The figure reflects the recommended energy scale correction due to a calibration correction, sample charging, flood gun, or other phenomenon.

Surf. Sci. Spectra, 28(2) Dec 2021; doi: 10.1116/6.0001146 - Published under an exclusive license by the AVS

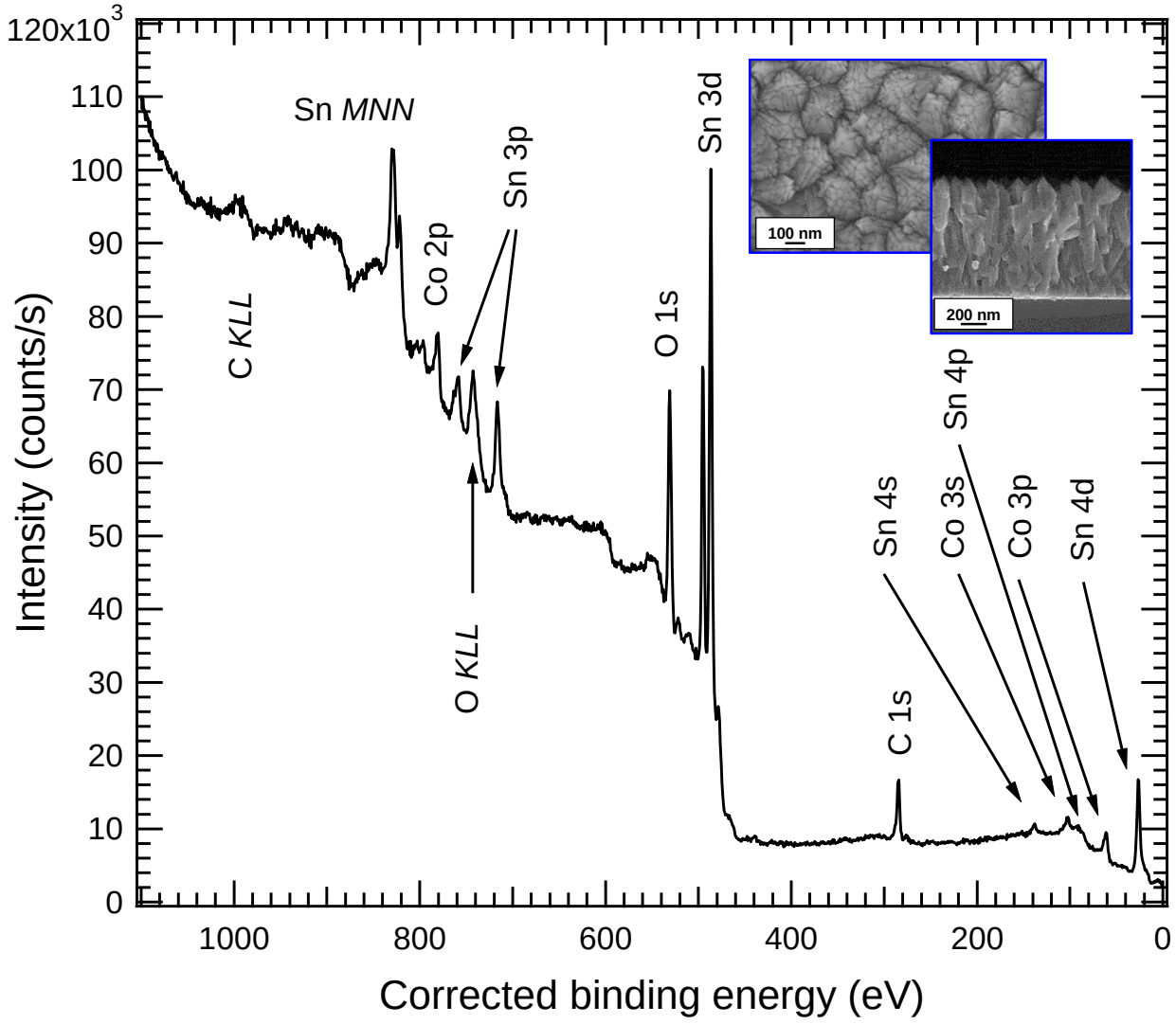

Publish in *Surface Science Spectra*: Yes ☒ No ☐

Accession #	NFigA01
Host Material	Co_3O_4-SnO_2
Technique	XPS
Spectral Region	survey
Instrument	Perkin-Elmer Physical Electronics, Inc. 5600ci
Excitation Source	Mg Ka
Source Energy	1253.6 eV
Source Strength	250 W
Source Size	>25 mm x >25 mm
Analyzer Type	spherical sector analyzer
Incident Angle	9˚
Emission Angle	45˚
Analyzer Pass Energy	187.85 eV
Analyzer Resolution	1.9 eV
Total Signal Accumulation Time	385.2 s
Total Elapsed Time	423.7 s
Number of Scans	14
Effective Detector Width	1.9 eV

Surf. Sci. Spectra, 28(2) Dec 2021; doi: 10.1116/6.0001146 - Published under an exclusive license by the AVS

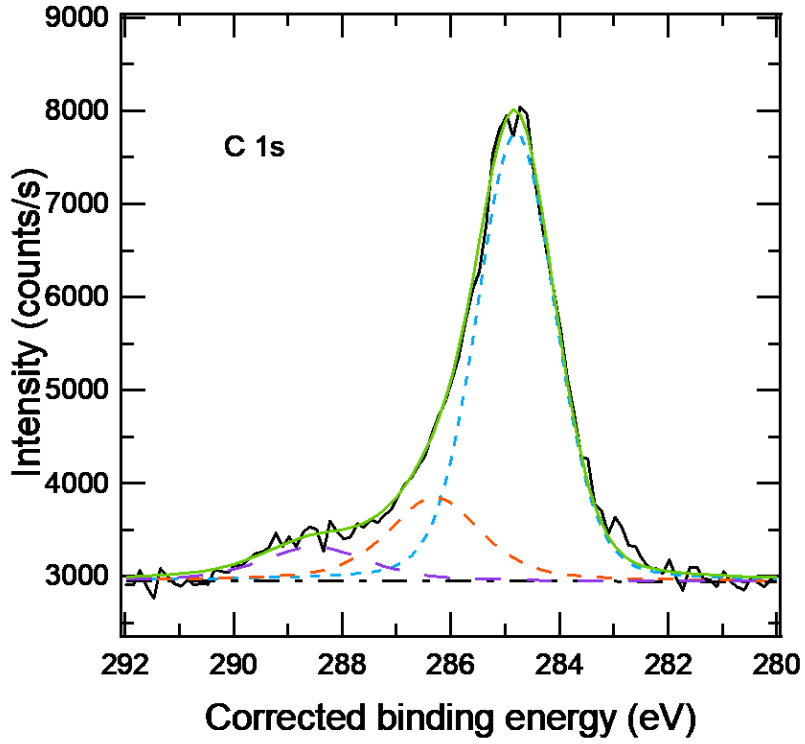

Publish in *SSS*: Yes ☒ No ☐

- **Accession #:** NFigA02
- **Host Material:** Co_3O_4-SnO_2
- **Technique:** XPS
- **Spectral Region:** C 1s

Instrument: Perkin-Elmer Physical Electronics, Inc. 5600ci
Excitation Source: Mg Ka
Source Energy: 1253.6 eV
Source Strength: 250 W
Source Size: >25 mm x >25 mm
Analyzer Type: spherical sector
Incident Angle: 9 °
Emission Angle: 45 °
Analyzer Pass Energy 58.7 eV
Analyzer Resolution: 0.6 eV
Total Signal Accumulation Time: 67.8 s
Total Elapsed Time: 74.6 s
Number of Scans: 12
Effective Detector Width: 0.6 eV

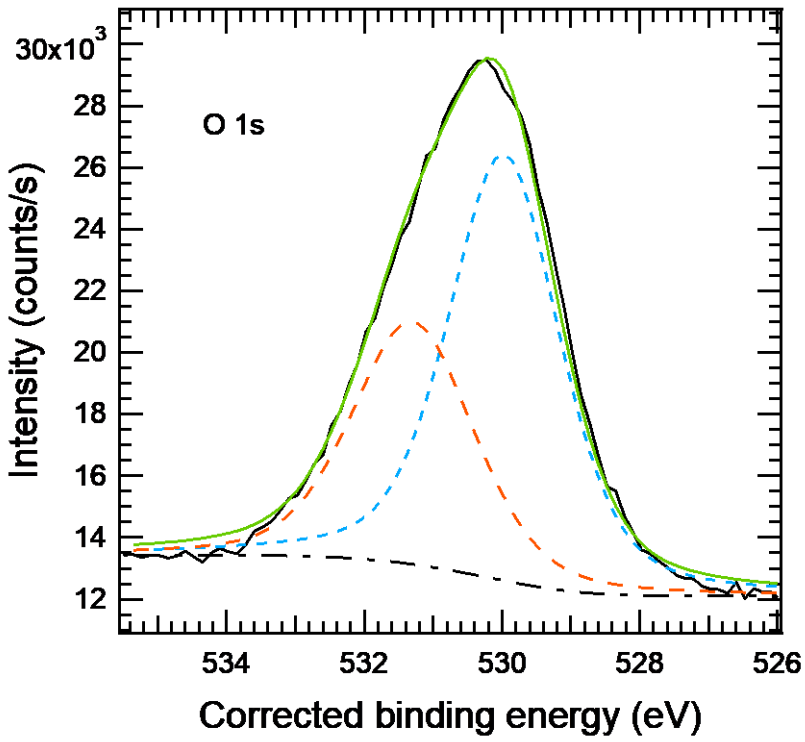

Publish in *SSS*: Yes ☒ No ☐

- **Accession #:** NFigA03
- **Host Material:** Co_3O_4-SnO_2
- **Technique:** XPS
- **Spectral Region:** O 1s

Instrument: Perkin-Elmer Physical Electronics, Inc. 5600ci
Excitation Source: Mg Ka
Source Energy: 1253.6 eV
Source Strength: 250 W
Source Size: >25 mm x >25 mm
Analyzer Type: spherical sector
Incident Angle: 9 °
Emission Angle: 45 °
Analyzer Pass Energy 58.7 eV
Analyzer Resolution: 0.6 eV
Total Signal Accumulation Time: 90.4 s
Total Elapsed Time: 99.4 s
Number of Scans: 16
Effective Detector Width: 0.6 eV

Surf. Sci. Spectra, 28(2) Dec 2021; doi: 10.1116/6.0001146 - Published under an exclusive license by the AVS

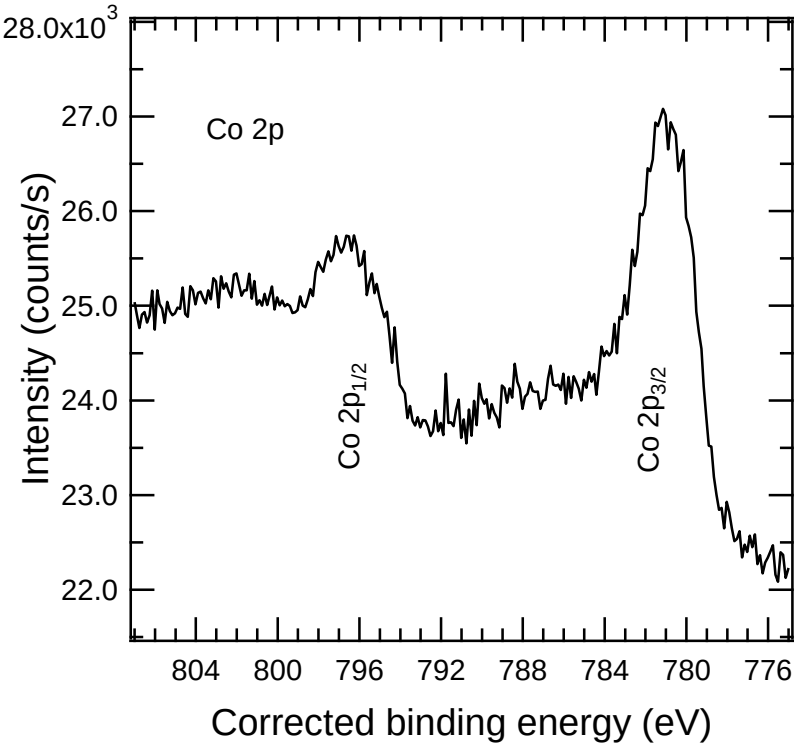

Publish in *SSS*: Yes ☒ No ☐

- **Accession #:** NFigA04.
- **Host Material:** Co_3O_4-SnO_2
- **Technique:** XPS
- **Spectral Region:** Co 2p

Instrument: Perkin-Elmer Physical Electronics, Inc. 5600ci
Excitation Source: Mg Ka
Source Energy: 1253.6 eV
Source Strength: 250 W
Source Size: >25 mm x >25 mm
Analyzer Type: spherical sector
Incident Angle: 9 ˚
Emission Angle: 45 ˚
Analyzer Pass Energy 58.7 eV
Analyzer Resolution: 0.6 eV
Total Signal Accumulation Time: 541.5 s
Total Elapsed Time: 595.6 s

Number of Scans: 30

Effective Detector Width: 0.6 eV

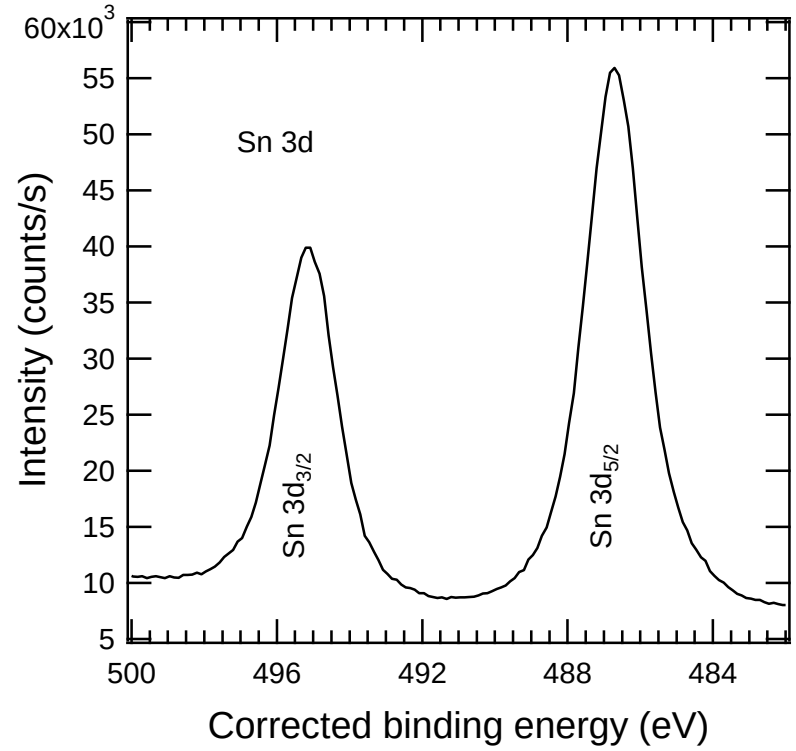

Publish in *SSS*: Yes ☒ No ☐

- **Accession #:** NFigA05.
- **Host Material:** Co_3O_4-SnO_2
- **Technique:** XPS
- **Spectral Region:** Sn 3d

Instrument: Perkin-Elmer Physical Electronics, Inc. 5600ci
Excitation Source: Mg Ka
Source Energy: 1253.6 eV
Source Strength: 250 W
Source Size: >25 mm x >25 mm
Analyzer Type: spherical sector
Incident Angle: 9 ˚
Emission Angle: 45 ˚
Analyzer Pass Energy 58.7 eV
Analyzer Resolution: 0.6 eV
Total Signal Accumulation Time: 180.9 s
Total Elapsed Time: 199.0 s

Number of Scans: 18

Effective Detector Width: 0.6 eV

Surf. Sci. Spectra, 28(2) Dec 2021; doi: 10.1116/6.0001146 - Published under an exclusive license by the AVS

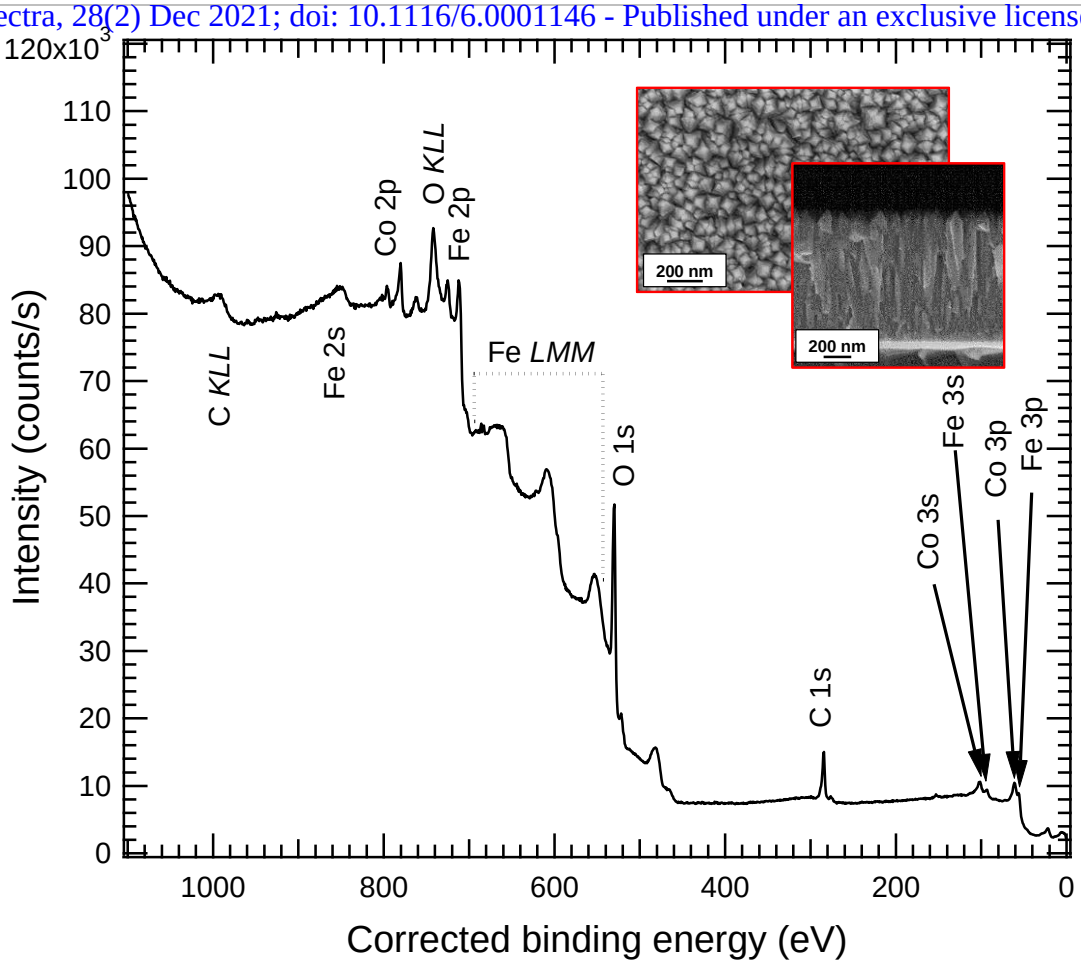

Publish in *Surface Science Spectra*: Yes ☒ No ☐

Accession #	NFigB01
Host Material	Co_3O_4-Fe_2O_3
Technique	XPS
Spectral Region	survey
Instrument	Perkin-Elmer Physical Electronics, Inc. 5600ci
Excitation Source	Mg Ka
Source Energy	1253.6 eV
Source Strength	250 W
Source Size	>25 mm x >25 mm
Analyzer Type	spherical sector analyzer
Incident Angle	9˚
Emission Angle	45˚
Analyzer Pass Energy	187.85 eV
Analyzer Resolution	1.9 eV
Total Signal Accumulation Time	2311.8 s
Total Elapsed Time	2543.0 s
Number of Scans	84
Effective Detector Width	1.9 eV

Surf. Sci. Spectra, 28(2) Dec 2021; doi: 10.1116/6.0001146 - Published under an exclusive license by the AVS

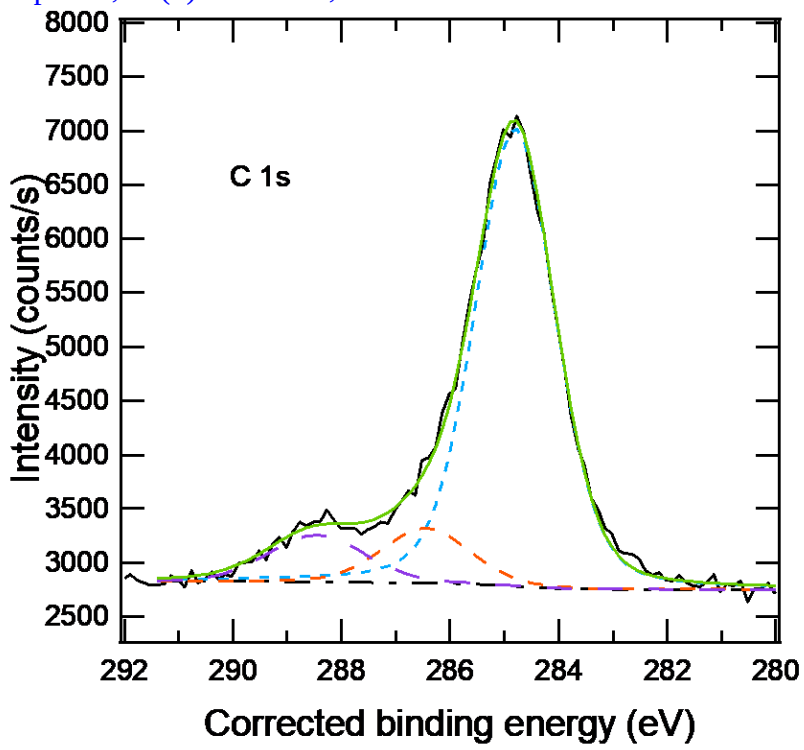

Publish in *SSS*: Yes X No ☐

- **Accession #:** NFigB02.
- **Host Material:** Co_3O_4-Fe_2O_3
- **Technique:** XPS
- **Spectral Region:** C 1s

Instrument: Perkin-Elmer Physical Electronics, Inc. 5600ci
Excitation Source: Mg Ka
Source Energy: 1253.6 eV
Source Strength: 250 W
Source Size: >25 mm x >25 mm
Analyzer Type: spherical sector
Incident Angle: 9 ˚
Emission Angle: 45 ˚
Analyzer Pass Energy 58.7 eV
Analyzer Resolution: 0.6 eV
Total Signal Accumulation Time: 123.3 s
Total Elapsed Time: 135.6 s

Number of Scans: 18

Effective Detector Width: 0.6 eV

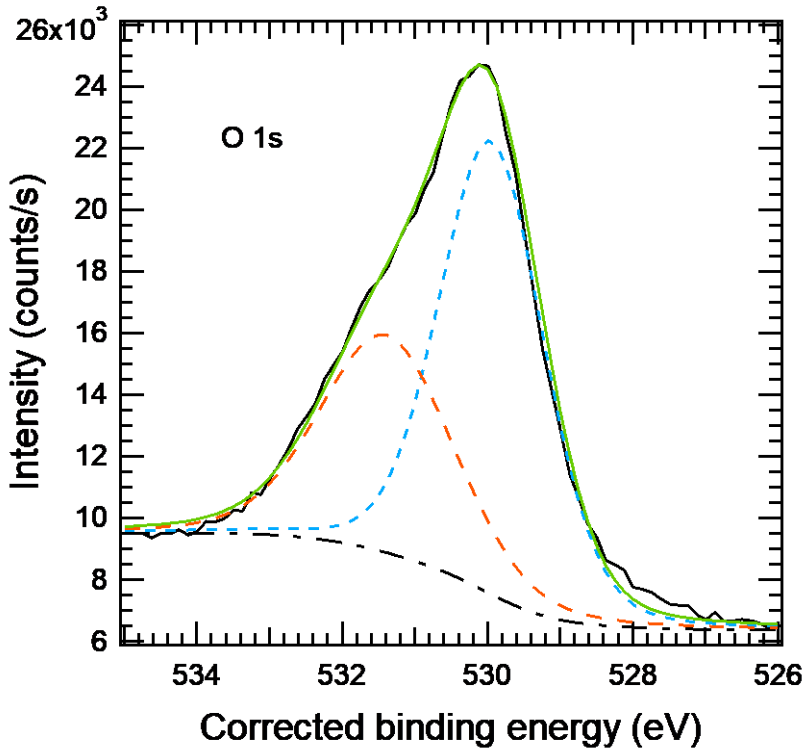

Publish in *SSS*: Yes X No ☐

- **Accession #:** NFigB03
- **Host Material:** Co_3O_4-Fe_2O_3
- **Technique:** XPS
- **Spectral Region:** O 1s

Instrument: Perkin-Elmer Physical Electronics, Inc. 5600ci
Excitation Source: Mg Ka
Source Energy: 1253.6 eV
Source Strength: 250 W
Source Size: >25 mm x >25 mm
Analyzer Type: spherical sector
Incident Angle: 9 ˚
Emission Angle: 45 ˚
Analyzer Pass Energy 58.7 eV
Analyzer Resolution: 0.6 eV
Total Signal Accumulation Time: 116.1 s
Total Elapsed Time: 127.7 s

Number of Scans: 18

Effective Detector Width: 0.6 eV

Surf. Sci. Spectra, 28(2) Dec 2021; doi: 10.1116/6.0001146 - Published under an exclusive license by the AVS

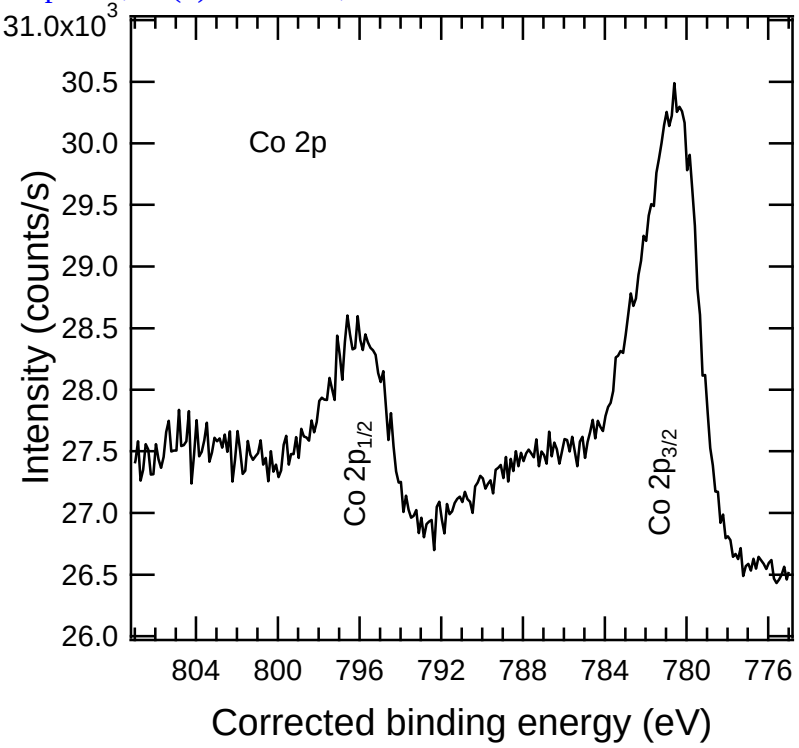

Publish in *SSS*: Yes X No ☐

- **Accession #:** NFigB04
- **Host Material:** Co_3O_4-Fe_2O_3
- **Technique:** XPS
- **Spectral Region:** Co 2p

Instrument: Perkin-Elmer Physical Electronics, Inc. 5600ci
Excitation Source: Mg Ka
Source Energy: 1253.6 eV
Source Strength: 250 W
Source Size: >25 mm x >25 mm
Analyzer Type: spherical sector
Incident Angle: 9 °
Emission Angle: 45 °
Analyzer Pass Energy 58.7 eV
Analyzer Resolution: 0.6 eV
Total Signal Accumulation Time: 1102.75 s
Total Elapsed Time: 1213.03 s

Number of Scans: 55

Effective Detector Width: 0.6 eV

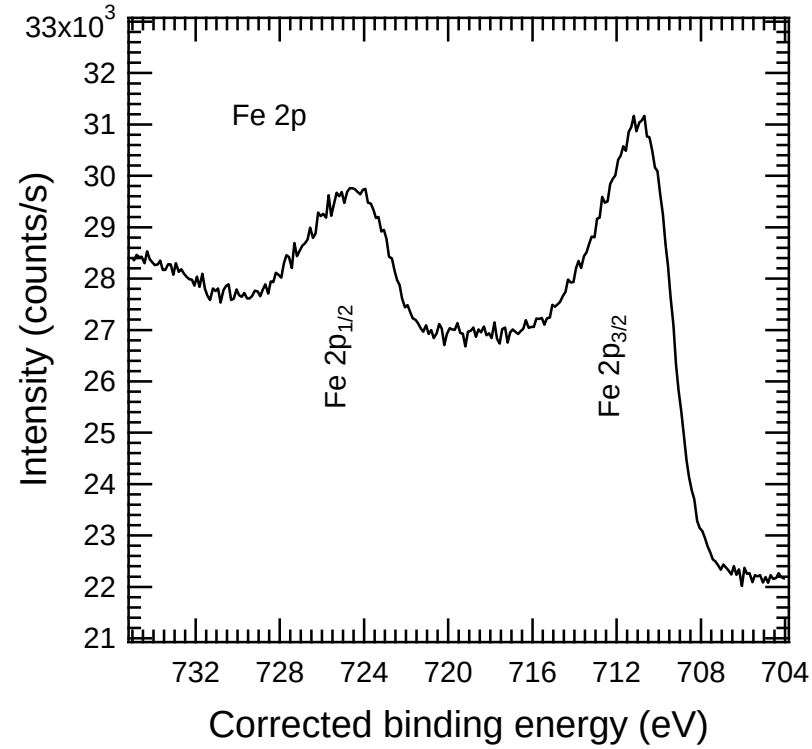

Publish in *SSS*: Yes X No ☐

- **Accession #:** NFigB05
- **Host Material:** Co_3O_4-Fe_2O_3
- **Technique:** XPS
- **Spectral Region:** Fe 2p

Instrument: Perkin-Elmer Physical Electronics, Inc. 5600ci
Excitation Source: Mg Ka
Source Energy: 1253.6 eV
Source Strength: 250 W
Source Size: >25 mm x >25 mm
Analyzer Type: spherical sector
Incident Angle: 9 °
Emission Angle: 45 °
Analyzer Pass Energy 58.7 eV
Analyzer Resolution: 0.6 eV
Total Signal Accumulation Time: 882.75 s
Total Elapsed Time: 971.03 s

Number of Scans: 55

Effective Detector Width: 0.6 eV